NACA



# RESEARCH MEMORANDUM

WIND-TUNNEL INVESTIGATION OF A WING-ROOT INLET CONFIGURATION WITH VARIOUS MODIFICATIONS AT

MACH NUMBERS OF 1.41, 1.81, AND 2.01

By A. Warner Robins

Langley Aeronautical Laboratory Langley Field, Va.

CLASSIFICATION CHANGE

CLASSIFIED DOCUMENT

This material contains information affecting the National Defense of the United States within the meaning of the espionage laws, Title 18, U.S.C., Secs. 793 and 794, the transmission or revelation of which in any manner to an unauthorized person is prohibited by law.

NATIONAL ADVISORY COMMITTEE FOR AERONAUTICS

WASHINGTON

September 26, 1957

To be returned to the files of the Named for Aeronautics

# NATIONAL ADVISORY COMMITTEE FOR AERONAUTICS

## RESEARCH MEMORANDUM

WIND-TUNNEL INVESTIGATION OF A WING-ROOT INLET

CONFIGURATION WITH VARIOUS MODIFICATIONS AT

MACH NUMBERS OF 1.41, 1.81, AND 2.01<sup>1</sup>

By A. Warner Robins

## SUMMARY

A wing-root inlet configuration in which inlet components were varied was tested in the Langley 4- by 4-foot supersonic pressure tunnel at Mach numbers of 1.41, 1.81, and 2.01 corresponding to Reynolds numbers per foot of  $4.19 \times 10^6$ ,  $3.74 \times 10^6$ , and  $3.46 \times 10^6$ , respectively. Angles of attack ranged from  $-4^\circ$  to  $15^\circ$  and a few configurations were tested in a sideslip range from  $-8^\circ$  to  $4^\circ$ . Inlet performance and engine-face flow distortions as affected by pitch, sideslip, inlet-lip sweep, contraction ratio, boundary-layer control, and engine bypass are presented and discussed.

## INTRODUCTION

An investigation of a twin-duct wing-root inlet installation designed for operation up to a Mach number of 2 and with provisions for variable supersonic compression and engine bypass has been made. The purpose of the investigation was to determine, at Mach numbers of 1.41, 1.81, and 2.01, the effects on inlet performance and engine-face total-pressure distributions of variations in angle of attack, sideslip, contraction ratio, and engine bypass, as well as to evaluate the effects of various modifications of the inlet itself.

The tests were conducted in the Langley 4- by 4-foot supersonic pressure tunnel at Mach numbers of 1.41, 1.81, and 2.01 and corresponding to Reynolds numbers per foot of 4.19  $\times$  10<sup>6</sup>, 3.74  $\times$  10<sup>6</sup>, and 3.46  $\times$  10<sup>6</sup>, respectively. The angles of attack were varied from -4° to 15°, and some configurations were tested in a sideslip range from -8° to 4°.

The information presented herein was previously made available to the U. S. military air services.

# SYMBOLS

A area at engine face

Ap inlet area projected on plane normal to fuselage axis

A+ area of inlet throat

H total pressure at engine face

Ho free-stream total pressure

- average area-weighted total pressure at engine face

 $\Delta H = H_{\text{max}} - H_{\text{min}}$ 

Mo free-stream Mach number

 $\frac{m}{m_O}$  mass-flow ratio,  $\frac{\rho AV}{\rho_O A_P V_O}$ 

V velocity at engine face

Vo free-stream velocity

α angle of attack

 $\beta$  angle of sideslip

ρ density at engine face

ρ<sub>0</sub> free-stream density

Subscripts:

max maximum

min minimum

## MODELS AND INSTRUMENTATION

## Models

A drawing of the basic wing-root inlet model, which was sting mounted in the tunnel, is shown in figure 1. The model consisted of the fuselage

forebody and stub wings (in which the twin inlets were located). In the layout of the model, provision was made for numerous changes in the inlet configuration including lip sweep, boundary-layer-diverter assembly, and contraction ratio. These and other variations are discussed in the following paragraphs.

Four sets of lips were investigated and are referred to in this paper as configurations 65/66 (the basic configuration shown in fig. 1), 58/66, 58/71, and 65/71 in which the first and second numbers refer to degrees of upper- and lower-lip sweep, respectively. A sketch of these lip configurations is presented in figure 2. Lip sweep is measured from the apex of each lip at fuselage station 20.40. Typical lip sections are shown in figure 3(b).

Some tests were performed with the 65/66 configuration with lip perforations consisting of twenty 3/32-inch holes drilled normal to the inlet surfaces near each of the four fuselage—inlet-lip junctures. The perforations were located in an area approximately 1/2 inch square. The centroids of these areas were approximately 1/2 inch behind the unswept portions of each of the inlet lips and approximately 1/4 inch outboard of the planes of the diverter plates.

Figure 4(a) shows the scheme of boundary-layer diverter-assembly operation. Figure 4(b) shows the diverter assemblies tested. The basic diverters are designated by letters A to F, whereas the various modifications are designated by the modification number which corresponds to the line code shown in figure 4(b). For example, diverter assembly El would be basic diverter assembly E with lengthened slots (modification 1) and diverter assembly E2,3 would be assembly E with modifications 2 and 3 but not modification 1; or assembly E with the most extreme bleed-exit flare. Slot widths of the slotted diverter assemblies were 0.046 inch. The tubing which formed the bleed system for diverter assembly B was of 0.040-inch inside diameter and provided that the air removed by each of the 0.040-inch-diameter perforations was individually dumped. The diverter wedges were set at -2.5° incidence with respect to the fuselage center line and were approximately 0.3 inch thick. This thickness was somewhat greater than the thickness of the fuselage boundary layer which was made turbulent for all tests by a transition strip of carborundum grains in shellac located as shown in figure 1.

Inlet contraction was varied between the limiting contours shown in figure 3(a). The system was designed for near-isentropic compression at the highest values of contraction ratios. Contraction ratios  $\frac{Ap}{At}$  for the present investigation were varied from 1.48 to 1.07.

Engine bypass was provided in each duct just ahead of the engineface station as shown in figure 1. Only fully open or fully closed bypass configurations were used in the tests.

7 July 1 87 and 2 01

# Instrumentation

The model was instrumented for pressure data only. Figure 1 shows the location of the engine-face total-pressure survey rake (station 36.76). The cross section at station 37.19 (fig. 1) shows the distribution of total-pressure tubes of the survey rake.

Mass flow was measured by a calibrated orifice plate located in the length of pipe into which the model ducting discharged. This piping can be seen in the photograph in figure 5. A remotely controlled, motordriven plug was located at the pipe discharge to provide for mass-flow control.

Schlieren photographs of the flow in the vicinity of the inlet were taken for most of the tests.

# Test Conditions

The investigation was made in the Langley 4- by 4-foot supersonic pressure tunnel with the following test conditions:

Mach number			•	•	•	•	•	•	•	•	•	•	•	•	•	•	•	•	Τ.	.41	- ,	Τ.	,01	- 9	and	1 Z.OI	
Reynolds numl	oer	ре	r	foo	ot	at	5:																	,		-6	
Reynolds number $M_0 = 1.41$								•		•			•				•	•	•		•			4.	19	× 10°	
M - 7 87																								3.	74	× 10°	
$M_0 = 2.01$						•	•	•		•		•	•	•	•	•	•	٠	•	•	•	•		2	40	X TO	
Stagnation p	res	sur	e.	a.	tm																					0.95	
Stagnation to	emp	era	tu	re	,	OF					•								•	•		•	•	•	•	100	

Transition on the fuselage was fixed for all tests by a strip of carborundum grains in shellac as shown in figure 1.

## RESULTS AND DISCUSSION

#### Presentation of Results

Figures 6 to 13 show pressure-recovery results for the basic configuration in pitch and sideslip and for various modifications of the inlet configuration in pitch at Mach numbers 1.41, 1.81, and 2.01. In these figures, the curves of  $\frac{\overline{H}}{H_0}$  plotted against  $\frac{m}{m_0}$  are carried to the lowest mass-flow rate for stable operation. Inlet instability was characterized by intermittent unstarting of either, or occasionally both, of the wing-root inlets. In the curves of  $\frac{\overline{H}}{H_0}$  plotted against  $\frac{m}{m_0}$ ,

there is generally no well-defined critical mass-flow point; therefore, operating points in the knee of the curve will be referred to as near-critical points. Contour plots of pressure recovery at the engine-face station are shown in figures 14 to 18. Engine-face total-pressure distortions at angles of attack for near-critical operating points are presented in figure 19. Figures 20, 21, and 22 present a representative set of schlieren photographs of the configuration operating at Mach numbers 1.41, 1.81, and 2.01.

## Discussion of Results

Performance results.- The effects of pitch and sideslip on the performance of the basic 65/66 configuration at  $M_0=2.01$  are shown in figure 6. As the angle of attack increased from  $0^{\circ}$  to  $15^{\circ}$ , maximum average total-pressure recoveries  $\overline{H}/H_0$  diminished from 0.83 to 0.68 and supercritical mass-flow ratios dropped from about 1.00 to 0.90. Maximum pressure recoveries for  $0^{\circ}$ ,  $\pm 4^{\circ}$ , and  $-8^{\circ}$  sideslip were about the same values (approximately 0.83) although near-critical mass-flow ratios were increased from approximately 0.95 to 1.00 when sideslip angle was increased from  $0^{\circ}$  and  $\pm 4^{\circ}$  to  $-8^{\circ}$ . The fact that pressure recoveries and mass flow did not diminish with increase in sideslip (fig. 6(b)) is attributed to the action of the fuselage vortices in thinning the fuselage boundary layer on the downstream side of the fuselage. The resultant pressure recovery in the downstream duct would probably be nearly the same as at  $0^{\circ}$  sideslip, and this condition, in conjunction with the higher pressure recovery incurred by the upstream inlet in a lower velocity field, would yield the favorable sideslip characteristics shown.

Pressure recoveries at angles of attack of -4°, 0°, 4°, 8°, 12°, and 15° for various lip sweeps are shown in figure 7. The complete lipsweep series with changes in lip sweep only was tested only at a Mach number of 1.81. The staggered-lip configurations were designed in an attempt to improve angle-of-attack performance of the inlet without appreciably penalizing recoveries at an angle of attack of 0°. The configuration (58/71) with the greatest stagger (differential sweep) showed the highest pressure recoveries at high angles of attack but exhibited very low recoveries at 0° and -4°. Of the two configurations with moderate stagger (58/66 and 65/71), the 58/66 configuration showed considerably less airhandling ability and lower total-pressure recoveries throughout the angleof-attack range. The 65/71 configuration showed increasingly higher recoveries than the 65/66 configuration from slightly above 00 through 15° angle of attack, although the pressure recoveries at 8°, 12°, and 15° were somewhat lower than those for the greatly staggered 58/71 configuration. In addition, the stable subcritical range of the 65/71 configuration exceeded that of all others tested.

Figure 8 indicates that increasing contraction ratio  $\rm Ap/A_t$  from the lowest value shown toward the theoretical ideal contraction ratio reduces inlet mass flow without affecting average total-pressure recovery. A contraction ratio of 1.43 appears desirable for Mach number 2.01. However, because of the large amount of throat boundary-layer air associated with the high ratio of inlet internal-surface area to inlet cross-section area and the low Reynolds number of the test, it appears that some boundary-layer bleed on the compression surfaces ahead of and at the inlet throat might permit higher contraction ratios and better overall inlet performance.

Various boundary-layer-diverter systems were tested at a Mach number of 2.01. Figure 9 shows the effects of varying the manner and amount of diverter bleed. Diverter assemblies BO, B, C, and C2 (see fig. 4), were applied to the 65/66 inlet configuration. No significant performance differences were found.

A comparison of inlet performance at a Mach number of 2.01 with the use of 40° and 60° diverter wedges is made in figure 10. Results of tests of diverter assemblies El and E2 and D, Dl, and F are shown. Bleed-exit flare varied in these configurations, the short-slot, 60° diverter assembly E2 having the largest amount of bleed-exit flare and the 40° diverter assemblies D and Dl having virtually none (see fig. 4). The effects of variation in bleed-exit flare are probably not significant. inasmuch as no performance differences were noted between configurations having the 40° diverter assemblies, Dl and F, with and without flare. In addition, tests of the 60° diverters with extreme exit flare at a different contraction ratio did not show any improvement in pressure recovery. When comparisons of the performances of the inlet with the 40° and 60° diverter assemblies are made, the 60° assembly appears to be slightly superior. More significant is the superiority of the short-slot diverter plates E2 and D in both the 40° and 60° diverter assemblies. The fact that the long bleed slots were less effective may be due, in part, to circulation within the long slots, the higher pressure air at the rear of the slots circulating through the bleed plenum and out at the forward end of the slots.

Figure 11 shows a comparison of recoveries measured with and without transition strips. These strips of no. 60 carborundum were placed within the inlet lips and on the diverter plate of the 65/66 configuration to insure turbulent boundary layers within the inlet. The transition strip on the diverter plate had virtually no effect. The strips within the lips, however, decreased inlet performance appreciably. It is believed that the carborundum grains used were too large and produced disturbances of sufficient size to thicken the boundary layer significantly. The fact that the maximum mass-flow ratio was decreased by 3 or 4 percent by this action indicates, as in the discussion of figure 8, that some amount of compression-surface boundary-layer bleed ahead of and at the inlet throat might be desirable.

Provision was made in the model to bypass a large amount of the inlet air on either side of the duct just ahead of the engine face. (See fig. 1.) The bypass doors were tested only in the fully opened and fully closed position. Figure 12 shows the performance of the 65/66 configuration with bypass doors opened and closed at Mach numbers of 1.81 and 2.01. In general, maximum recoveries with the bypass doors open were about the same as those for which the doors were closed. Mass flows at these recoveries were reduced by 20 to 25 percent. Inlet instability occurred in the same way for the configuration with bypass as in the case of no bypass, that is, either one, or occasionally both, of the wing-root inlets would intermittently become unstarted.

The tests of the inlet at a Mach number of 1.41 were limited to the determination of the effect of varying inlet contraction ratio from 1.19 to 1.07 on the performance of a modified 65/66 inlet with diverter assembly E2. The modification of the 65/66 inlet lips was minor and consisted of the extension of all but the outer 15 percent of each of the inlet lips by 0.08 inch normal to the lip leading edges. The outer 15 percent of each lip was tapered from the new lip line to the original lip apex at model station 20.40. The performance of the inlet for the two contraction ratios is shown in figure 13. Pressure recoveries for the two conditions are approximately the same but the inlet with the highest degree of inlet contraction appears to be spilling about 10 percent of the inlet air.

Perforations in the inboard sections of the lips were made in an attempt to increase the range of stable subcritical operation. The results of this modification (not presented) indicated no effect on either stable operating range or pressure recovery and a decrease of the order of 2 percent in inlet mass flow.

Engine-face pressure recovery contours.— Figures 14 to 18 show contour plots of local total-pressure recovery  $\rm H/H_{O}$  at the engine face as seen looking downstream. An interval of 0.04 between contour lines is used throughout these figures. For each test condition, plots for supercritical, near-critical and, where available, subcritical mass-flow ratios are shown. Corresponding performance plots may be found in figures 6 to 13.

Figure  $1^4$  shows the effects of inlet contraction on engine-face total-pressure-recovery distribution for the 65/66 inlet configuration at an angle of attack of  $0^\circ$  and Mach number 2.01. Although inlet contraction had an appreciable effect on inlet mass flow (see fig. 8), no significant effect on engine-face flow distortion is noted.

Figure 15 shows the effect of sideslip on the distribution of local total-pressure recovery at the engine face for the 65/66 configuration at Mach number 2.01. Throughout the mass-flow range, the total-pressure distributions for the configuration at -8° sideslip were comparable to

8

or better than those for the lower sideslip angles. The corresponding inlet performance plot is shown in figure 6(b).

NACA RM L57A28

A comparison at an angle of attack of 0° of engine-face total-pressure-recovery distribution for the 65/66 configuration at Mach number 2.01 for various means and amounts of diverter plate bleed is shown in figure 16. For all but the lowest mass-flow ratios, the amount and manner of diverter-plate bleed shown do not significantly affect flow distortion. At the lowest mass-flow ratio, however, the configuration without bleed exhibited the least engine-face flow distortion.

Figure 17 shows the effects of open bypass doors on engine-face total-pressure-recovery distributions for the 65/66 configurations at Mach number 2.01 at angles of attack of 0°, 8°, and 15°. These total-pressure-recovery contours correspond to the performance data shown in figure 12. The highest mass-flow points resulted in extreme distortions to the point of flow separation in the duct just downstream of each bypass door. It is believed that, since these distortions are a function of normal-shock position in the diffuser, similar distortions might be experienced with bypass doors closed. At the lowest mass-flow ratio with bypass doors fully open, flow distortion is comparable to the low mass-flow distortions for the configuration with bypass doors closed.

Figure 18 shows the effect of lip sweep on engine-face total-pressure-recovery distribution at  $0^{\circ}$  and  $15^{\circ}$  angle of attack at Mach number 1.81. For the configurations with  $8^{\circ}$  or more of differential in lip sweep, flow distortion is considerably reduced when angle of attack is increased from  $0^{\circ}$  to  $15^{\circ}$ . At an angle of attack of  $15^{\circ}$ , for these configurations, the variation in flow distortion with mass flow is unsystematic and small. With the 65/66 configuration, however, distortion diminishes with decrease in mass flow and, for near-critical mass flow, no reduction in distortion is exhibited with an increase of angle of attack to  $15^{\circ}$ .

Figure 19 presents the effects of angle of attack on engine-face total-pressure distortions  $\frac{\Delta H}{H}$  of the 65/66, 58/66, 58/71, and 65/71

configurations for near-critical inlet operating points at Mach number 1.81. The numerator  $\Delta H$  is the difference between the maximum and minimum total pressures measured by the engine-face survey rake. Distortions for the configurations with lip stagger generally tend to diminish from  $-4^{\circ}$  to  $15^{\circ}$  angle of attack. The unstaggered or 65/66 configuration shows a minimum distortion level near  $4^{\circ}$  and high distortions at both  $-4^{\circ}$  and  $15^{\circ}$  angle of attack. Maximum distortion is found at  $-4^{\circ}$  angle of attack for the configuration with maximum lip stagger. The least variation and the lowest overall level of distortion is seen for the 65/71 configuration.

Schlieren observations. - Figures 20, 21, and 22 show representative schlieren photographs of the basic configuration (65/66) operating at an angle of attack of 0° at Mach numbers 1.41, 1.81, and 2.01, respectively.

The photographs in figure 20 are for the 65/66 configuration which was modified as mentioned previously in the discussion of performance at Mach number 1.41. Because the mass flow for this configuration at Mach number 1.41 exceeded the capacity of the metering equipment, only near-critical and subcritical points are shown. In these photographs no separated boundary layer is noted on the diverter plate.

The photographs in figure 21 are for the basic configuration (65/66) for supercritical and near-critical operation at Mach number 1.81. The inlets were not operating identically. The inlet shown in the upper part of the photograph showed boundary-layer separation beginning at or slightly ahead of the boundary-layer bleed slots in the diverter plate. Separation is not apparent on the inlet shown in the lower part of the photograph. The photograph on the right (m/mo = 0.93) shows a vortex sheet the path of which (toward diverter plate) indicates appreciable air flow through the bleed slots.

Schlieren photographs of the inlet operating at Mach number 2.01 are shown in figure 22. The shock which had produced the boundary-layer separation at Mach number 1.81 is now seen to fall farther back or on the canceling or expansion region of the diverter plate where the pressure gradient would be less favorable to separation. Some separation is evident, however, at the lowest mass-flow point shown. It should be noted that inlet operation with and without diverter-plate bleed was comparable at a Mach number of 2.01. (See fig. 9.)

Thus, from schlieren observations of inlet operation at Mach numbers of 1.41, 1.81, and 2.01 and performance results at Mach number 2.01, it appears that provisions for bleeding off the diverter-plate boundary layer in order to avoid thickened or separated boundary layers due to shock boundary-layer interactions might be helpful at the lowest and highest Mach numbers and might actually be a requirement for efficient inlet operation in the intermediate speed range. At a Mach number of 1.81 some improvement in inlet operation might result from compartmenting the bleed plenum to avoid circulation within the slots, as appears to be evident in the two schlieren photographs for the higher mass flows in figure 21, and extending forward the diverter-plate slots to bleed ahead of the separation-producing shock seen for the lowest mass-flow point in figure 21.

## CONCLUSIONS

A wing-root inlet model in which inlet components were varied was tested at Mach numbers 1.41, 1.81, and 2.01 and corresponding Reynolds numbers per foot of  $4.19 \times 10^6$ ,  $3.74 \times 10^6$ , and  $3.46 \times 10^6$ , respectively. Angles of attack ranged from  $-4^\circ$  to  $15^\circ$ . One configuration was tested

in sideslip from  $-8^{\circ}$  to  $4^{\circ}$  at Mach numbers 1.81 and 2.01. The data indicate the following conclusions:

- l. Tests of inlets with varying degrees of lip sweep showed that some inlet-lip stagger improved pressure recoveries at high angles of attack with little or no compromise in characteristics at an angle of attack of 0°. Total-pressure profiles at the engine face are similarly improved by lip stagger.
- 2. Inlet performance and engine-face total-pressure-recovery distributions were not adversely affected by increase of sideslip to the maximum angle tested.
- 3. Inlet contraction ratio appears to have a significant effect on the maximum mass-flow rate but, within the range tested, a negligible effect on total-pressure recovery and engine-face total-pressure-recovery distributions. At the Reynolds numbers of these tests, use of a contraction ratio considerably less than the theoretical value is indicated to be desirable.
- 4. Maximum pressure recoveries with the engine bypass doors fully open approximated those for the configuration with the bypass doors closed. Mass flows at these recoveries were reduced 20 to 25 percent.

Langley Aeronautical Laboratory,
National Advisory Committee for Aeronautics,
Langley Field, Va., January 8, 1957.

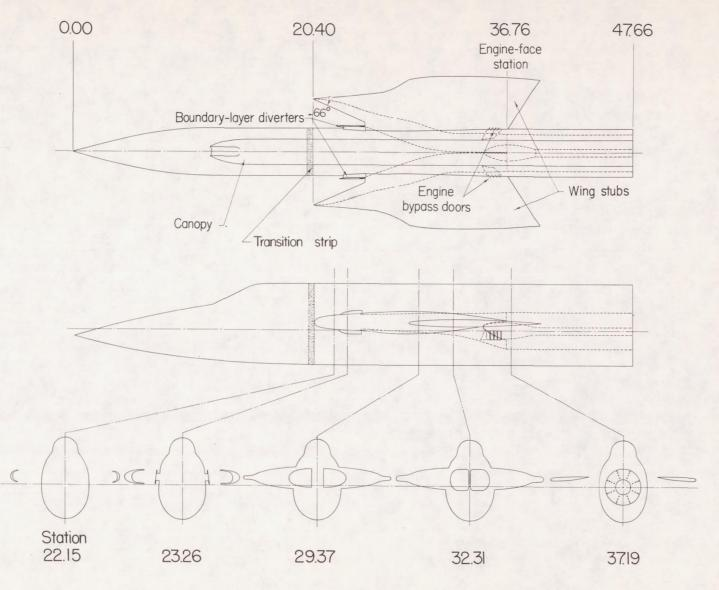
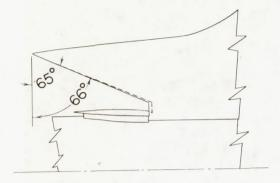
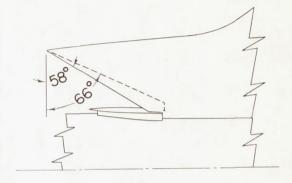


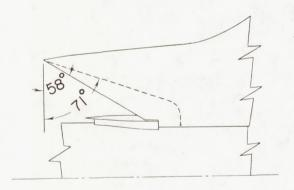
Figure 1.- Sketch of basic model. All dimensions are in inches.



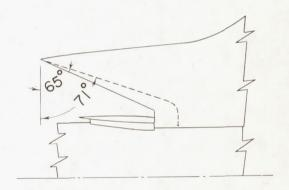
Configuration 65/66



Configuration 58/66

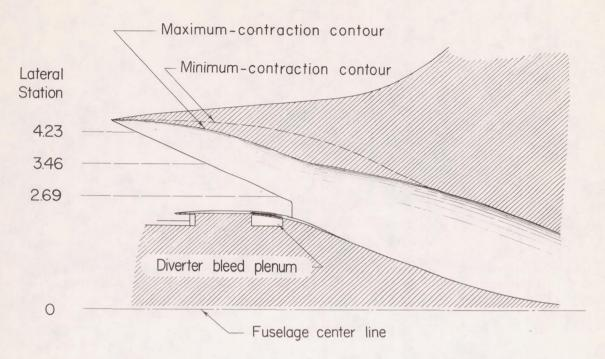


Configuration 58/71

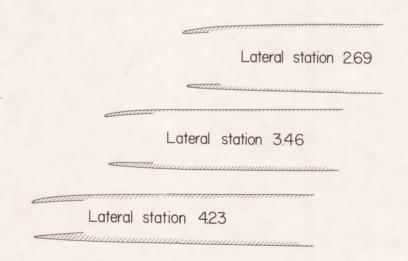


Configuration 65/71

Figure 2.- Sketches of inlet-lip configurations investigated. (Top view shown.)

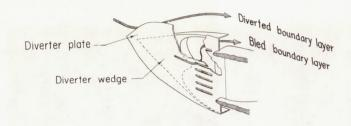


(a) Right inlet section parallel to yaw plane 0.661 inch above fuselage center line.

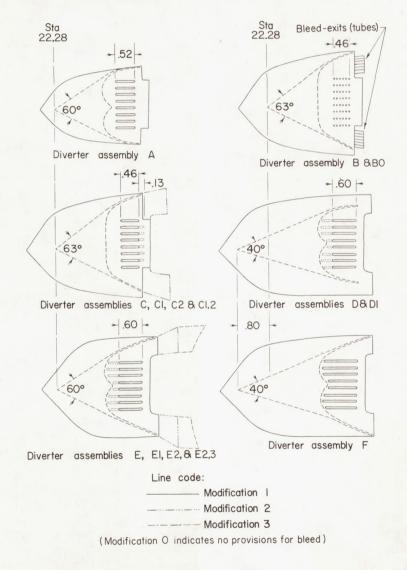


(b) Partial chordwise sections through right inlet showing lip shapes at several lateral stations.

Figure 3.- Details of wing-root inlet. Configuration 65/66 with diverter assembly A shown. All dimensions in inches.



(a) Scheme of diverter-assembly operation.



(b) Layout and identification of diverter assemblies.

Figure 4.- Details of boundary-layer-diverter assemblies. All dimensions are in inches.

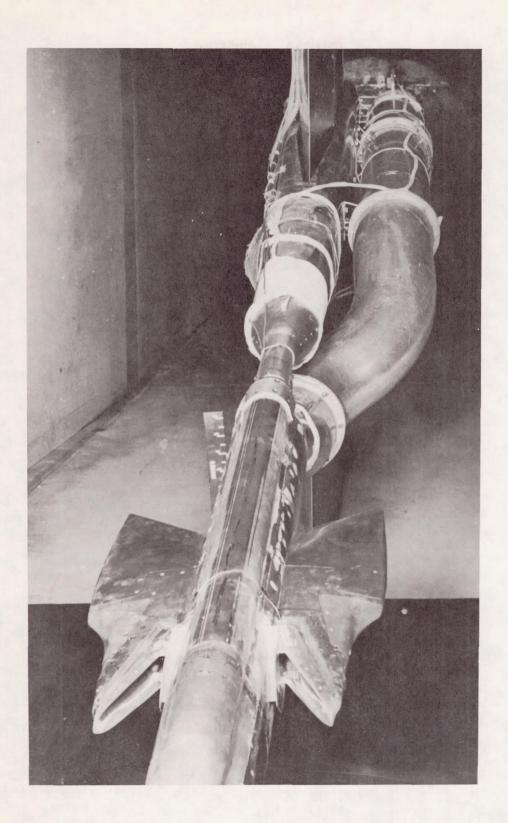
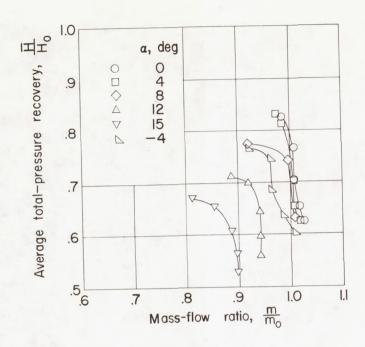
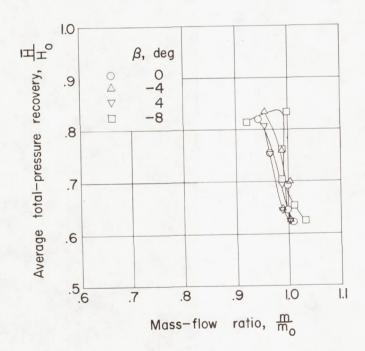


Figure 5.- Photograph of model in tunnel.

CONFIDENTIAL



(a) Effects of angle of attack at  $\beta = 0^{\circ}$ .



(b) Effects of sideslip at  $\alpha = -0.2^{\circ}$ .

Figure 6.- Effects of pitch and sideslip on performance of the 65/66 configuration with diverter assembly A at  $M_{\odot}$  = 2.01 and Ap/At = 1.48.

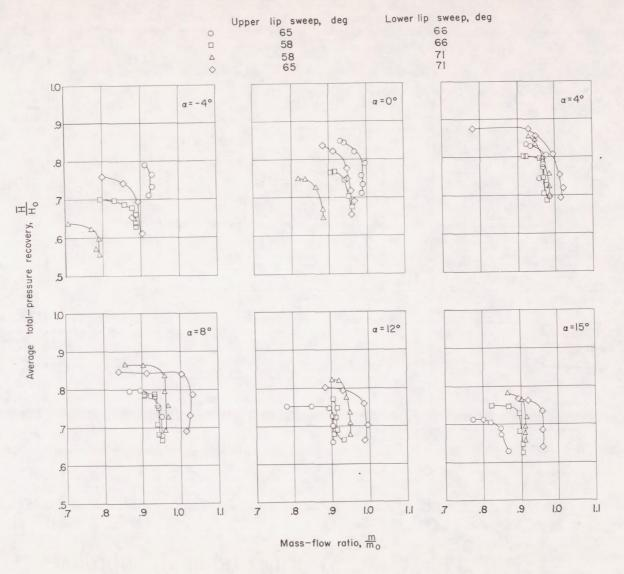


Figure 7.- Inlet performance throughout the angle-of-attack range of configurations of various lip sweeps at  $M_{\rm O}$  = 1.81 with diverter assembly A and Ap/At = 1.32.

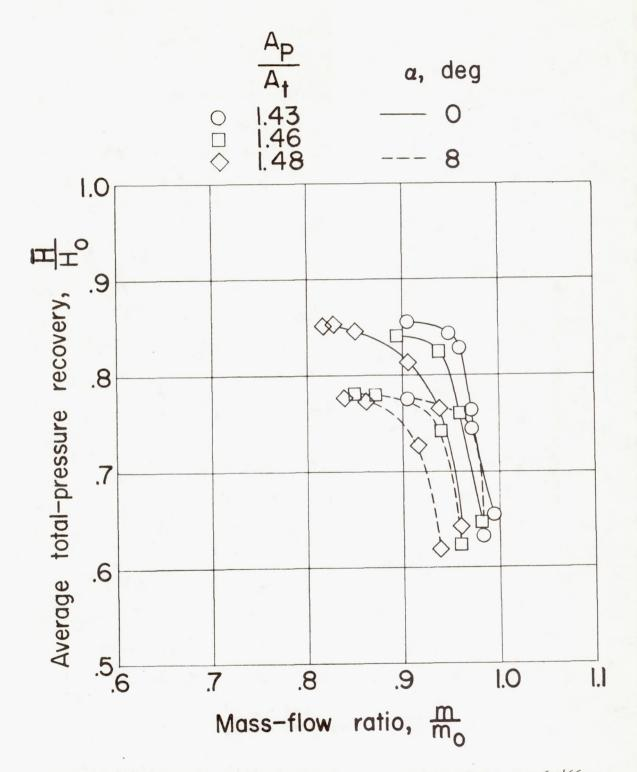


Figure 8.- Effect of contraction ratio on performance of the 65/66 configuration with diverter assembly E2 at  $M_0$  = 2.01.

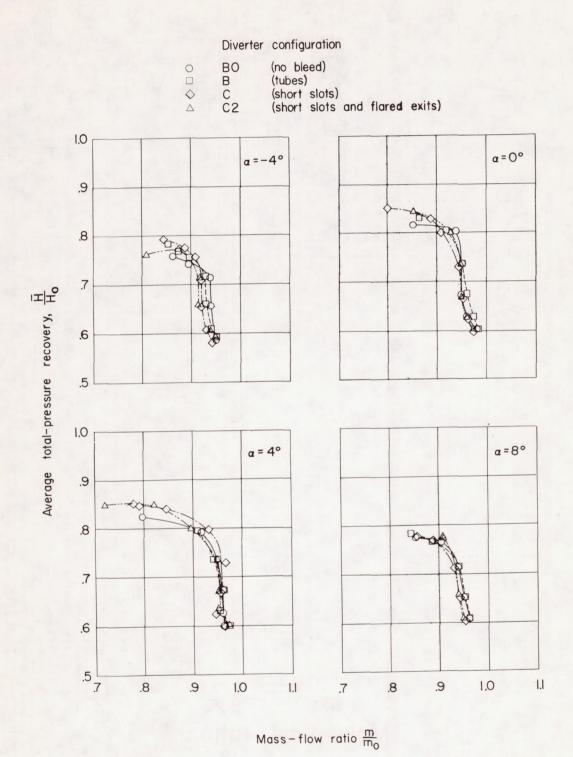


Figure 9.- Performance of 65/66 configuration with various diverter-assembly configurations at  $M_{\rm O}$  = 2.01 and Ap/At = 1.48.

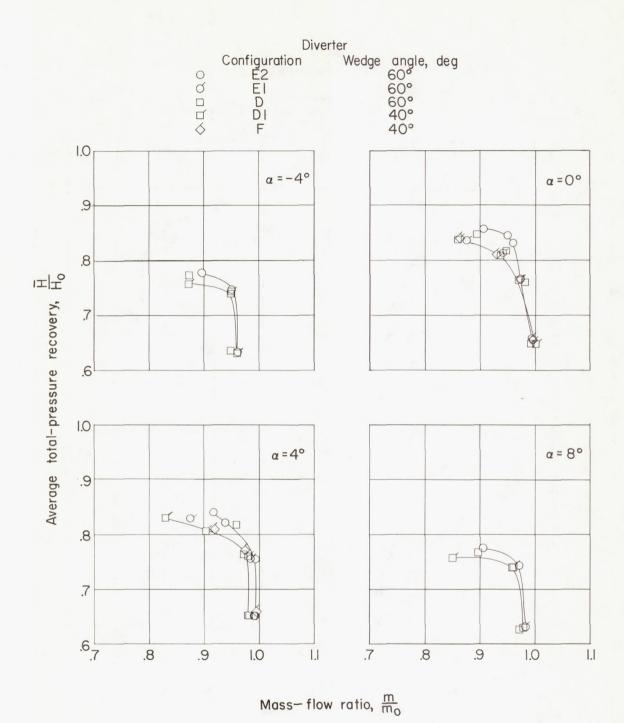


Figure 10.- Inlet performance for 65/66 configuration with diverters of  $40^{\circ}$  and  $60^{\circ}$  wedge at  $M_{o}$  = 2.01 and  $A_{P}/A_{t}$  = 1.43. (Tailed symbols indicate long diverter-plate bleed slots.)

- No transition strips
- □ Transition on diverter plate
- Transition inside lips

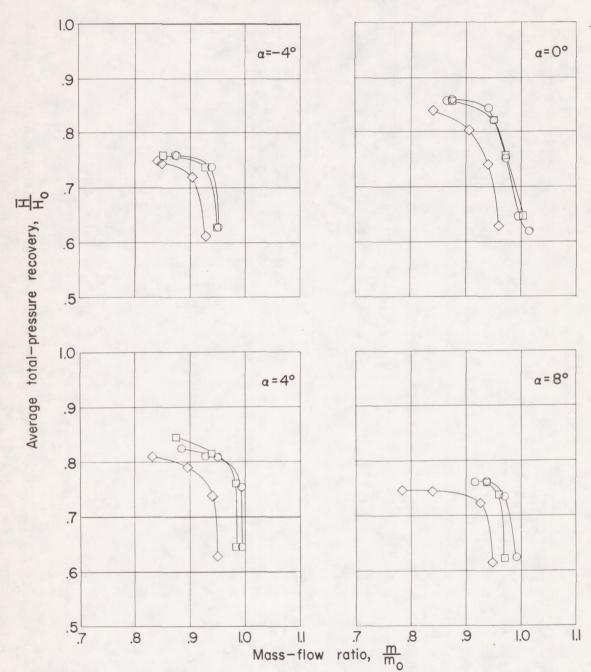


Figure 11.- Effect of transition strips on performance of the 65/66 configuration with diverter assembly C1,2 at  $M_{\odot}$  = 2.01. and Ap/At = 1.43.

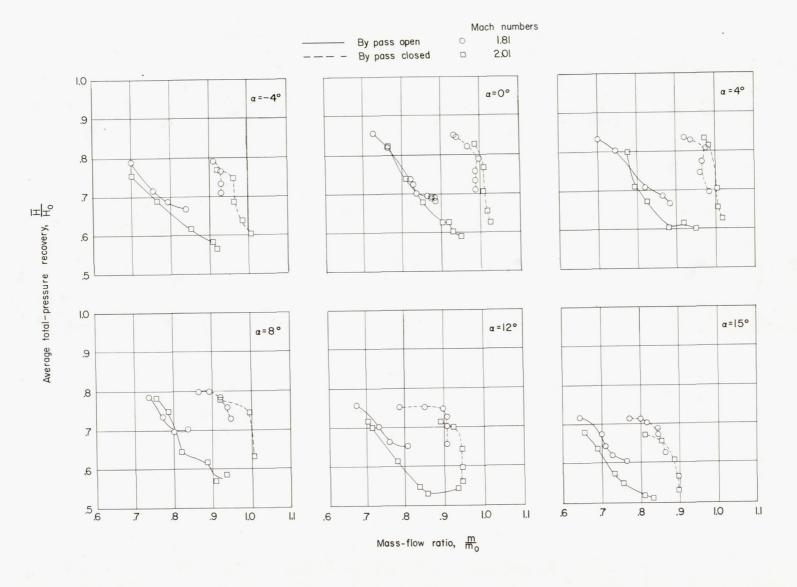


Figure 12.- Performance of the 65/66 configuration with diverter assembly A for open and closed bypass doors.  $A_P/A_t = 1.32$  at  $M_O = 1.81$  and  $A_P/A_t = 1.48$  at  $M_O = 2.01$ .

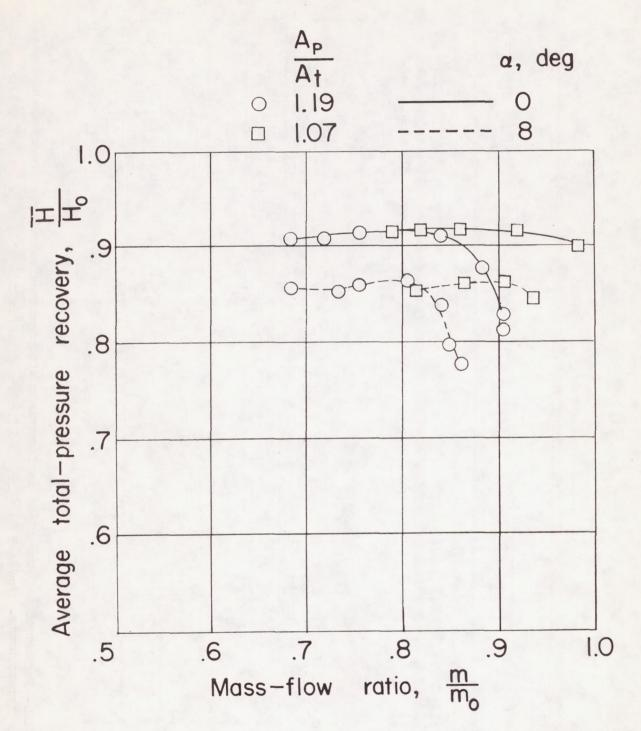


Figure 13.- Performance of the 65/66 configuration with modified lips and diverter assembly E2 at  $M_{\rm O}$  = 1.41.

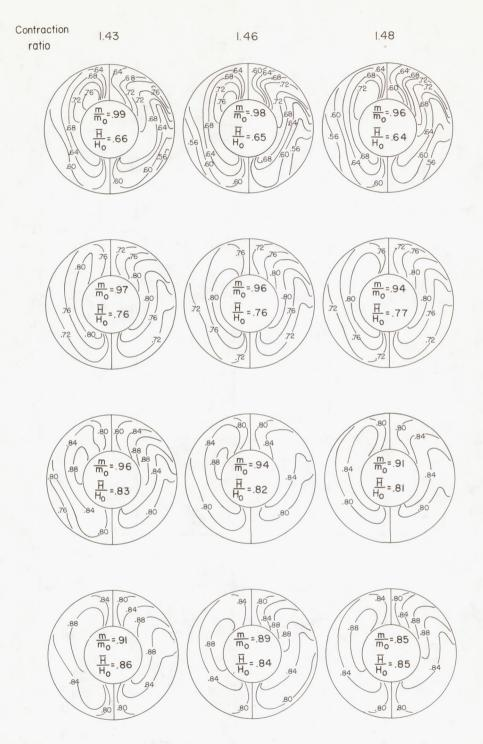


Figure 14.- Effect of contraction ratio on engine-face total-pressure-recovery distributions for the 65/66 configuration with diverter assembly E2 at  $M_{\rm O}$  = 2.01 and  $\alpha$  = 0°.

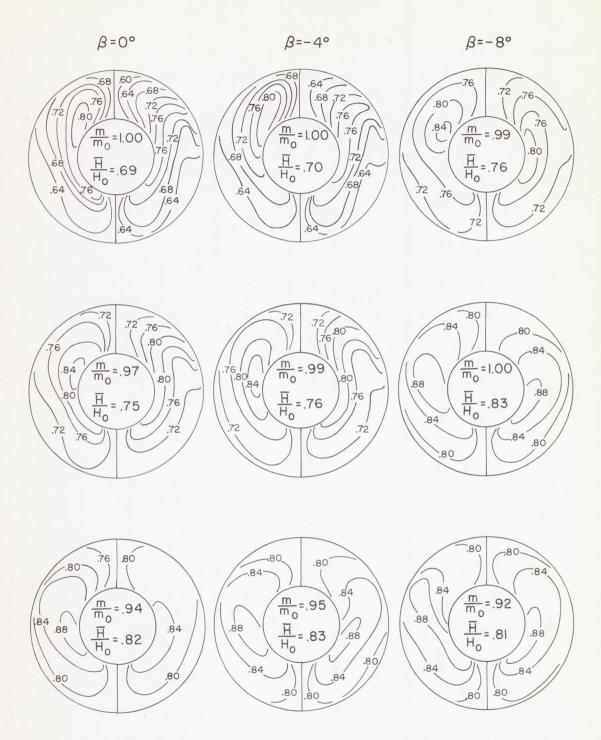


Figure 15.- Effect of sideslip on engine-face total-pressure-recovery distributions for the 65/66 configuration with diverter assembly A at M<sub>O</sub> = 2.01, Ap/A<sub>t</sub> = 1.48 and  $\alpha$  = -0.2°.

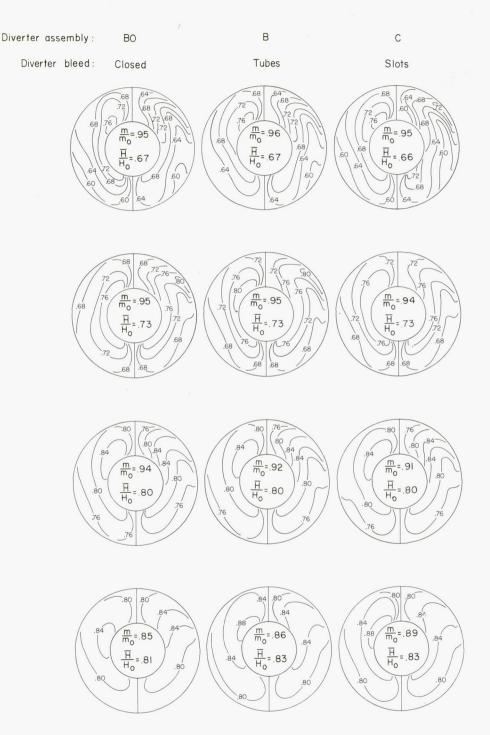


Figure 16.- Effect of diverter-plate bleed configuration on the engine-face total-pressure-recovery distributions for the 65/66 inlet configuration at  $\rm M_O$  = 2.01, Ap/At = 1.43 and  $\alpha$  = 0°.

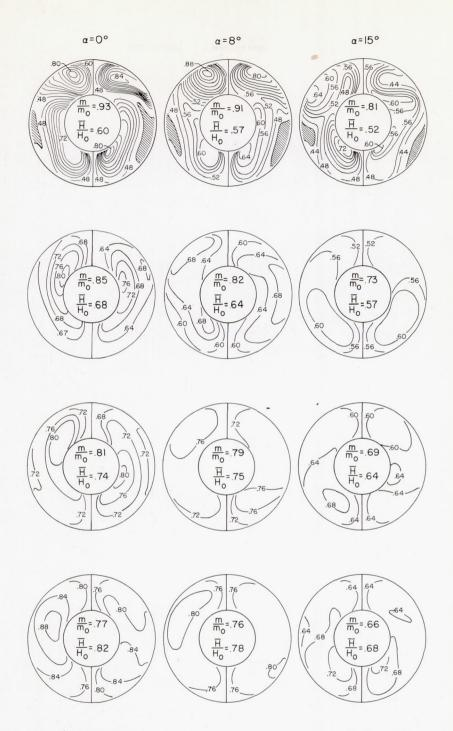


Figure 17.- Engine-face total-pressure-recovery distributions at various angles of attack for the 65/66 inlet configuration with diverter assembly A and with bypass doors open. Ap/At = 1.48 and  $M_O$  = 2.01. (Shaded areas indicate separated flow.)

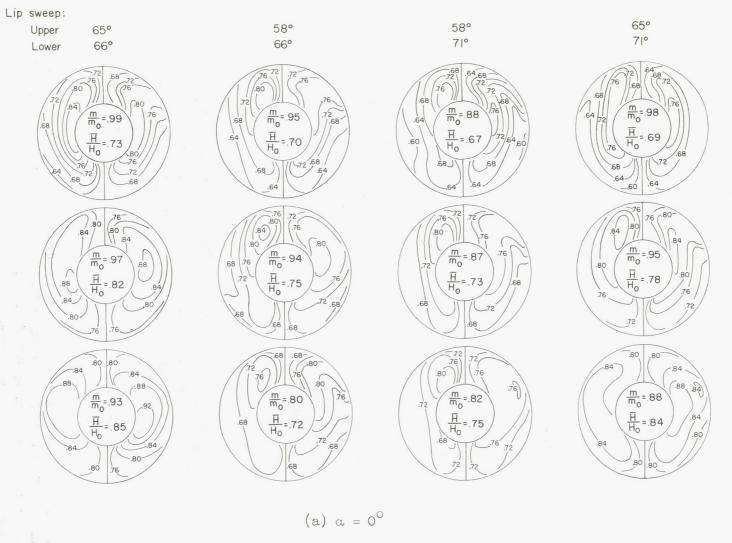


Figure 18.- Effect of lip sweep on engine-face total-pressure-recovery distribution with diverter assembly A and at  $M_O$  = 1.81 and  $Ap/A_t$  = 1.32.

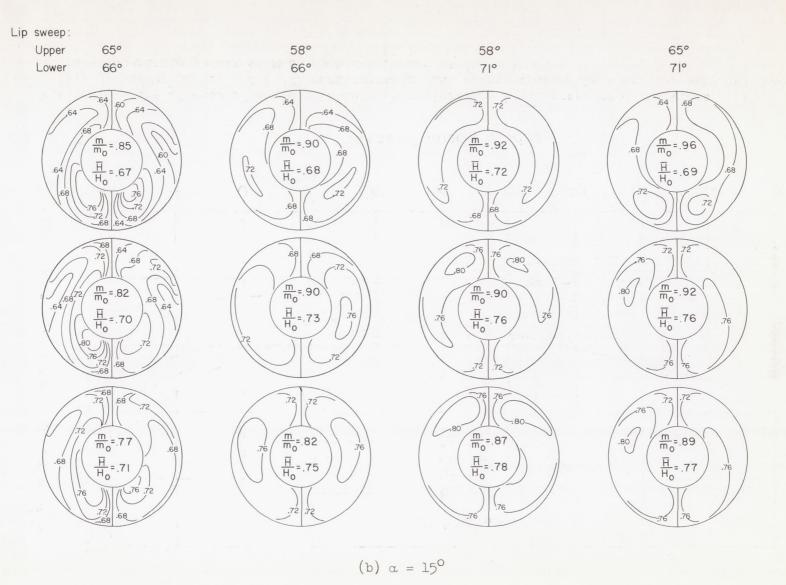


Figure 18. - Concluded.

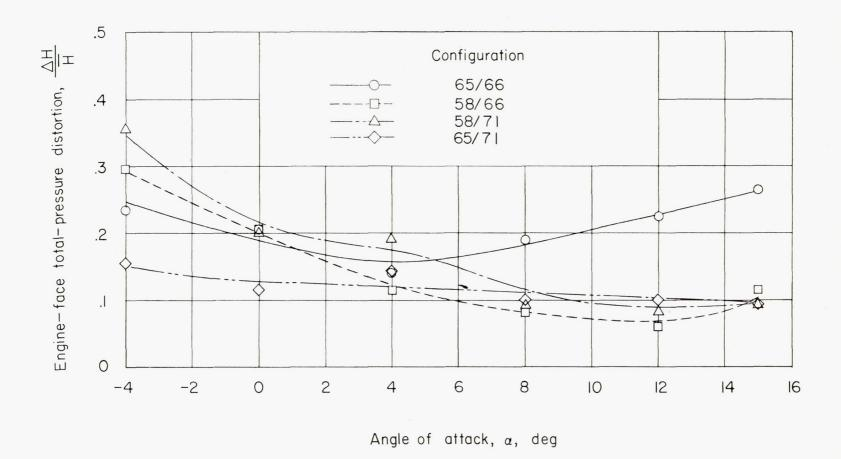
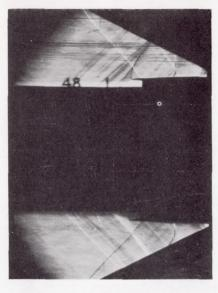
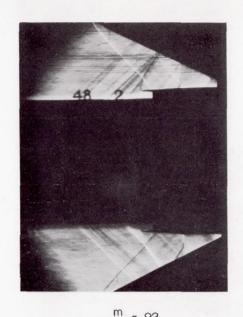


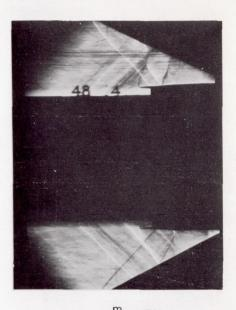
Figure 19.- The effects of angle of attack on engine-face total-pressure distortions of the 65/66, 58/66, 58/71, and 65/71 configuration with diverter assembly A and for near critical inlet operating points at Mach number 1.81 and  $A_P/A_t = 1.32$ .



 $\frac{m}{m_0} = .98$   $\frac{\overline{H}}{H_0} = .90$ 

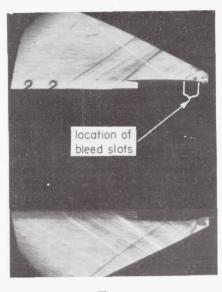


 $\frac{m}{m_0} = .92$   $\frac{\overline{H}}{H_0} = .92$ 



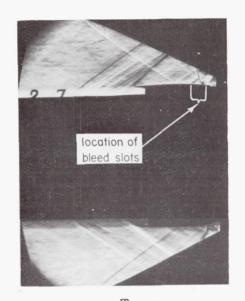
 $\frac{m}{m_0} = .79$   $\frac{\overline{H}}{H_0} = .91$ 

Figure 20.- Schlieren photographs at  $M_0$  = 1.41 of the modified 65/66 configuration with diverter E2 and  $A_P/A_t$  = 1.07 at  $\alpha$  = 0°. (Top view shown.)



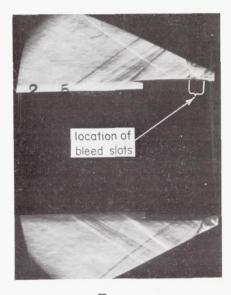
$$\frac{m}{m_0} = .99$$

$$\frac{\overline{H}}{H_0} = .71$$



$$\frac{m}{m_0} = .98$$

$$\frac{\overline{H}}{H_0} = .73$$



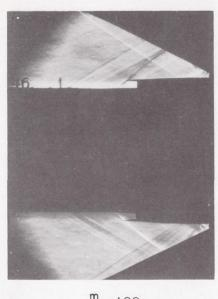
$$\frac{m}{m_0} = .93$$

$$\frac{\overline{H}}{H_0} = .85$$

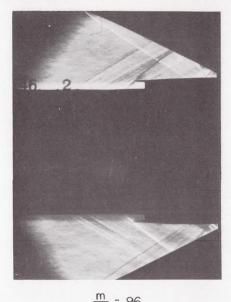
L-57-123

Figure 21.- Schlieren photographs at  $M_0$  = 1.81 of inlet configuration 65/66 with diverter A and  $A_P/A_t$  = 1.32 at  $\alpha$  = 0°. (Top view of inlet shown.)

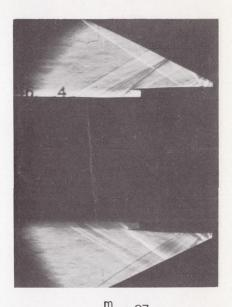
NACA RM 157A28



 $\frac{m}{m_0} = 1.00$   $\frac{\overline{H}}{H_0} = .66$ 



 $\frac{m}{m_0} = .96$   $\frac{\overline{H}}{H_0} = .77$ 



 $\frac{m}{m_0} = .93$   $\frac{\overline{H}}{H_0} = .85$ 

L-57-124 Figure 22.- Schlieren photographs at  $M_0 = 2.01$  of inlet configuration 65/66 with diverter E2,3 and  $A_P/A_t = 1.46$  at  $\alpha = 0^{\circ}$ . (Top view of inlet shown.)